GOOGLE EARTH ENGINE: APPLICATION OF ALGORITHMS FOR REMOTE SENSING OF CROPS IN TUSCANY (ITALY)

J. P. Clemente[1,2,*], G. Fontanelli[3], G. G. Ovando[1], Y. L. B. Roa[2,4], A. Lapini[3], E. Santi[3]

[1] Universidad Nacional de Córdoba. Facultad de Ciencias Agropecuarias, Córdoba, Argentina -(jpclemente, gugovan)@agro.unc.edu.ar
[2] Instituto de Altos Estudios Espaciales Mario Gulich (CONAE-UNC), Córdoba, Argentina
[3] Institute of Applied Physics-National Research Council, Firenze, Italy - (gfontanel,a.lapini,e.santi)@ifac.cnr.it
[4] CONICET and Instituto CEDIAC, Universidad Nacional de Cuyo, Mendoza, Argentina - yelob3@gmail.com

KEY WORDS: Google Earth Engine, Support Vector Machine, Crop classification, Random Forest, Sentinel-1, Sentinel-2

ABSTRACT:

Remote sensing has become an important mean to assess crop areas, specially for the identification of crop types. Google Earth Engine (GEE) is a free platform that provides a large number of satellite images from different constellations. Moreover, GEE provides pixel-based classifiers, which are used for mapping agricultural areas. The objective of this work is to evaluate the performance of different classification algorithms such as Minimum Distance (MD), Random Forest (RF), Support Vector Machine (SVM), Classification and Regression Trees (CART) and Naïve Bayes (NB) on an agricultural area in Tuscany (Italy). Four different scenarios were implemented in GEE combining different information such as optical and Synthetic Aperture Radar (SAR) data, indices and time series. Among the five classifiers used the best performers were RF and SVM. Integrating Sentinel-1 (S1) and Sentinel-2 (S2) slightly improves the classification in comparison to the only S2 image classifications. The use of time series substantially improves supervised classifications. The analysis carried out so far lays the foundation for the integration of time series of SAR and optical data.

1. INTRODUCTION

Food security is a broad concept that goes beyond production since it requires accounting for spatial and temporal variability of food availability, as well as physical and economic access. Accurate and continuous information on food production are essential to food producers, traders and consumers. In order to collect relevant data and to gain firsthand knowledge about the domestic and international agricultural situations, many countries and institutions around the world developed dedicated agriculture monitoring systems by complementing their traditional ground-based approach with satellite remote sensing based inputs (Wu et al., 2015).

Optical and microwave remote sensing technologies have become an important mean for extracting crop information at local and global scale (Sun et al., 2019; Belward, Skøien, 2015).

Traditionally, remote sensing for agricultural applications has focused mainly on optical data, acquired at the visible and near-infrared part of the electromagnetic spectrum (Orynbaikyzy et al., 2019). Nowadays, with the advancement in sensor technology and processing capability, it is possible to expand methodological approaches and use complementary data sources as satellite Synthetic Aperture Radar (SAR) imagery.

Van Tricht et al. (2018) used the integration of radar Sentinel-1 (S1) and optical Sentinel-2 (S2) images and an optimized Random Forest (RF) classifier to create a crop map for Belgium. They concluded that the synergistic use of radar and optical data increases classification accuracies in crop mapping compared to optical-only classification.

*Corresponding author

Sun et al. (2019) compared three advanced machine learning algorithms such as Support Vector Machine(SVM), Artificial Neural Network (ANN), and Random Forest for crop mapping on a test area in Yangzi River in China using scenes from S1, S2 and Landsat-8 (L8). The authors concluded that the combination of the three satellite data provided the best overall accuracy and Random Forest resulted to be the best classifier.

Recently Google Earth Engine (GEE) has been used on a wide range of Earth observation activities as i) land cover mapping of Continental Africa by integrating pixel-based and object-based algorithms using S2 and L8 data (Xiong et al., 2017), ii) paddy rice mapping in north eastern Asia using L8 images, (Dong et al., 2016), iii) deriving cropland extent product of Australia and China (Teluguntla et al., 2018), iv) evaluating combinations of temporally aggregated S1, S2 and L8 for land cover mapping (Carrasco et al., 2019), v) testing the performances of S1 data for classifying croplands (Mirelva, Nagasawa, 2019), vi) land cover classification in Lesotho using machine learning and S2 data (Mardani et al., 2019).

Agriculture in Italy faces problems and challenges as to mention calamities, drought, ungulates and predators and deficient management of the Community Agricultural Policy and the Rural Development Program. The Tuscany Council of the Italian Confederation of Agriculturist (2017) issued an alert about the heavy situation of the Tuscan agricultural enterprises, which is very critical in all the productive sectors. Some initiatives have been taken by local, regional and national workforces, but, to date, results have been disappointing. The consequence is land abandonment and the closure of farms.

The aim of this research is to develop a classification methodology based on Google Earth Engine and free satellite images provided by the ESA S1 and S2 constellations. This classification methodology will be the first step to implement an operative monitoring of agricultural practices, land degradation and will also provide tools for regional rural agencies in support of decision making and rural development programming.

2. MATERIALS AND METHODS

2.1 Study area

The study area is located in the south of Empoli and west of Florence, in the Tuscany region (Italy). The central coordinate is 43°39'33"N, 10°57'22"E, as shown in Figure 1.

It is a flat area, crossed by the Elsa river and surrounded by low and mild hills cropped with olive, vineyards and grass. The main crops are wheat, maize, sunflower and fava bean.

2.2 Field data

The land cover data was downloaded from the website of the Sistema Informativo Territoriale ed Ambientale (2019). A mask was built in order to exclude rivers, urban areas, forests and roads from crop classification.

Field campaigns were conduced from February 2019 to September 2019, where different crop types were identified and vectorized as Regions of Interest (ROI) (Figure 1).

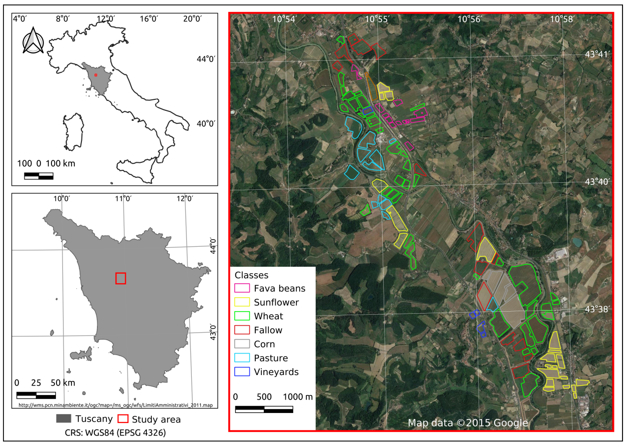

Figure 1. Regions of interest selected during the 2019 *in situ* measurement campaigns. Map data © 2015 Google

The most represented classes of vegetation described during the campaigns are listed below and were used for the classifications as shown in Table 1.

Classes	Number of polygons	Area (m^2)	Number of pixels
Fava beans	11	2121245	212124
Corn	5	1435953	143595
Wheat	39	2848868	284887
Vineyards	5	799831	79983
Fallow	14	2584841	258484
Pasture	12	2402975	240298
Sunflower	21	2618176	261818

Table 1. Agricultural classes used for crop classification of the test area

2.3 Cloud platform for imagery supplying and classification

The research described in this paper was carried out using Google Earth Engine (GEE). This cloud infrastructure allows us to access and seamlessly process large amount of freely available satellite imagery, including those acquired by the L8, S2 and S1 (Gorelick et al., 2017).

GEE also provides a set of the state-of-the-art tools for pixel-based classification that can be used for crop mapping (Shelestov et al., 2017).

2.4 Satellite data

S1 and S2 satellite images from GEE were used individually or together, depending on the scenario applied. The S2 scenes were atmospherically corrected using sen2cor (Müller-Wilm et al., 2019). The S1 scenes were calibrated and geocoded using the S1 Toolbox (ESA, 2019).

The S2 2, 3, 4, 5, 6, 7 and 8 bands and the S1 VV and VH backscatter and incidence angle bands were used according to the scenario applied. In Table 2 it is shown the SAR and optical images used.

Date	Sensor	Passage	Date	Sensor	Passage
2019-06-01	S1	Asc	2019-02-13	S2	Des
2019-06-05	S1	Des	2019-02-23	S2	Des
2019-06-13	S1	Asc	2019-03-20	S2	Des
2019-06-18	S1	Asc	2019-03-25	S2	Des
2019-08-12	S1	Asc	2019-03-30	S2	Des
2019-09-04	S1	Asc	2019-04-19	S2	Des
2019-09-04	S1	Des	2019-06-03	S2	Des
2018-09-26	S2	Des	2019-06-13	S2	Des
2018-10-21	S2	Des	2019-06-18	S2	Des
2018-11-15	S2	Des	2019-08-12	S2	Des
2018-12-25	S2	Des	2019-09-01	S2	Des
2019-01-04	S2	Des	2019-09-11	S2	Des

Table 2. SAR and optical images used in different scenarios. Descending (Des), Ascending (Asc)

Also Optical and SAR indices were derived and used for the classification, as shown in Table 3.

Vegetation Index (VI)	Abbreviation	Reference
Normalized Difference VI	NDVI	Bilal et al. (2019)
Enhanced Vegetation Index	EVI	Bilal et al. (2019)
Green-Red VI	GRVI	Motohka et al. (2010)
Simple Ratio Red-Green	SSRG	Gamon and Surfus (1999)
VH/VV Ratio	VH/VV	Fieuzal et al. (2013)

Table 3. Vegetation indices derived from optical and SAR information

2.5 Supervised Classification

The supervised classifiers Minimum Distance (MD) (Jony et al., 2018), Random Forest (RF) (Breiman, 2001), Support Vector Machine (SVM) (Burges, 1998; Mathur, Foody, 2008; Kumar et al., 2015), Classification and Regression Trees (CART) (Bishop, 2006; Shelestov et al., 2017), Naïve Bayes (NB) (Haykin, 2009; Shelestov et al., 2017) available from the GEE were used and tested in this work.

This contribution has been peer-reviewed.
https://doi.org/10.5194/isprs-archives-XLII-3-W12-2020-291-2020 | © Authors 2020. CC BY 4.0 License.
Primary publication at IEEE Xplore: https://doi.org/10.1109/LAGIRS48042.2020.9165561

2.6 Statistical analysis

A confusion matrix was derived for each classification test. From each matrix the global or overall accuracy (*GA*) and *Kappa* index (k) were calculated.

GA compares the number of correct predictions (pixels correctly classified) and reference pixels based on ground truth (Rwanga, Ndambuki, 2017).

k represents the degree of accuracy of image classification. k statistic ranges between zero and one, where k index equal to one means perfect agreement (Jog, Dixit, 2016). The scale proposed by Monserud and Leemans (1992) was used to interpret the k values.

2.7 Scenario workflow

Four different scenarios were implemented in GEE to classify individual images or time series, as shown in Figure 2.

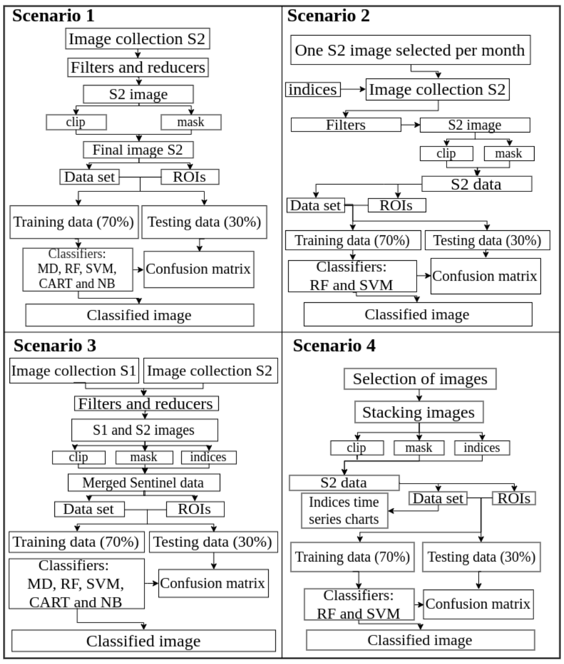

Figure 2. Different scenarios implemented in GEE

3. RESULTS AND DISCUSSION

3.1 Scenario 1

Scenario 1 assessed the classification accuracy of different algorithms using only individual S2 images. Bands 2, 3, 4, 5, 6, 7, and 8 were used. Scenes that gave the best results were 2019-06-03 and 2019-08-12, as shown in Figure 3.

Among all the classifiers applied to the selected images in the scenario 1, the only case that obtained fair values of k (0.48) was SVM using the 2019-06-03 S2 scene, with 58% of *GA*. Then, the following in performance were RF and CART, that reached a poor degree of agreement for k. For all the images analysed MD and NB had the lowest performances, since they did not exceed 44% of *GA*.

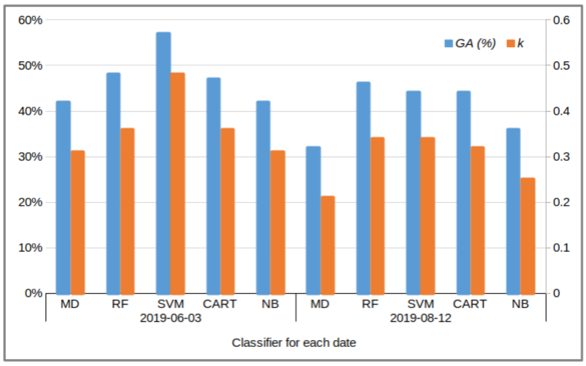

Figure 3. Comparison of *GA* and k for each classifier and date used in Scenario 1

3.2 Scenario 2

In this scenario only S2 images were used for the classification. In order to improve the classification accuracy, bands 2, 3, 4, 5, 6, 7 and 8 were coupled by NDVI, GRVI, EVI and SSRG indices.

In general, images from September, October, November and December 2018 showed low classification k degrees of agreement. This is because agricultural vegetation was harvested or just seeded. Of the 22 classifications applied to the 11 images, only four exceeded 60% of *GA* as shown in Figure 4.

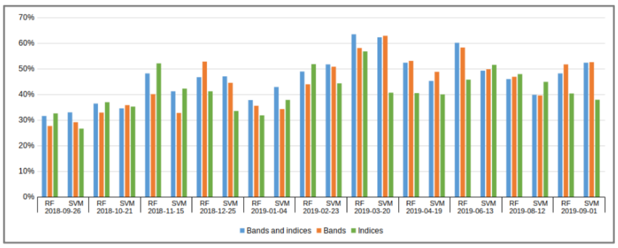

Figure 4. Comparison of *GA* for each classifier and date used in Scenario 2

The best performances were obtained for the 2019-03-20 scene, where RF (bands and indices) and SVM (bands) obtained values of 63% of *GA* and good values of k (Table 4).

Maps of the classification results for 2019-03-20 scene obtained with RF (bands and indices) and SVM (bands) are presented in Figure 5.

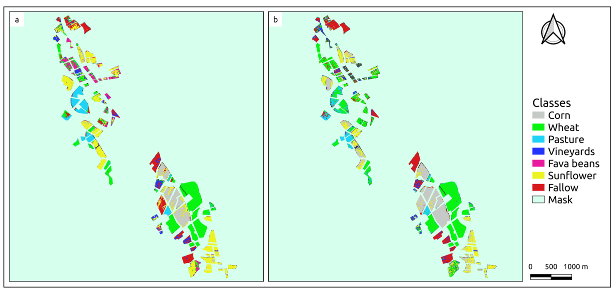

Figure 5. Classified Images in Scenario 2. a) RF for the date 2019-03-20 with bands and indices. b) SVM for the date 2019-03-20 with bands (Scenario 2)

Data	Scenario	Bands and indices	Bands	indices
		k	k	k
2018-09-26	RF	0.15	0.10	0.16
	SVM	0.17	0.13	0.01
2018-10-21	RF	0.19	0.15	0.21
	SVM	0.16	0.18	0.12
2018-11-15	RF	0.36	0.26	0.41
	SVM	0.28	0.16	0.26
2018-12-25	RF	0.35	0.42	0.29
	SVM	0.34	0.34	0.12
2019-01-04	RF	0.24	0.21	0.17
	SVM	0.31	0.23	0.24
2019-02-23	RF	0.38	0.32	0.42
	SVM	0.43	0.41	0.31
2019-03-20	RF	0.56	0.50	0.48
	SVM	0.53	0.54	0.26
2019-04-19	RF	0.44	0.45	0.29
	SVM	0.35	0.39	0.25
2019-06-13	RF	0.50	0.48	0.34
	SVM	0.39	0.39	0.38
2019-08-12	RF	0.34	0.35	0.37
	SVM	0.29	0.29	0.31
2019-09-01	RF	0.35	0.39	0.26
	SVM	0.41	0.41	0.20

Table 4. k index for RF and SVM classifiers applied to different dates and using combinations of bands and/or indices in Scenario 2

3.3 Scenario 3

In the scenario 3 the integration of different inputs corresponding to one optical and one radar image for crop mapping was tested. The combinations of images are presented in Table 5.

Test	Integration of images
1	S1: 2019-06-01, Asc. S2: 2019-06-03
2	S1: 2019-06-05, Des. S2: 2019-06-03
3	S1: 2019-06-13, Asc. S2: 2019-06-13
4	S1: 2019-06-18, Asc. S2: 2019-06-18
5	S1: 2019-08-12, Asc. S2: 2019-08-12
6	S1: 2019-09-04, Asc. S2: 2019-09-01
7	S1: 2019-09-04, Des. S2: 2019-09-01

Table 5. Integration of images used for scenario 3

Among all the combinations of input data the two best performing are presented in Table 6, where it is shown the *GA* and k values for the Test 3 and 4.

The highest performance was obtained for Test 3, where optical bands, optical indices along with SAR backscatter and incidence angle were used. In this case 63% of *GA* was obtained with good k values.

3.4 Scenario 4

The scenario 4 tested the classification accuracy using time series (TS) of S2 bands (bands 2, 3, 4, 5, 6, 7, 8) and indices (EVI, SSRG, GRVI) acquired in key periods of the 2019 Italian agricultural year (Table 7).

The algorithm uses image time series to improve the discrimination among different classes with respect to the classification carried out on single images. The discriminating capacity of time series can be appreciated in Figure 6, where the time evolution of the median EVI of each class is reported.

Since SVM and RF showed better performances in the previous scenarios only these two were used in this case.

In general, classifications using time series provided better results than previous scenarios. In all cases they were higher than 55.5% of *GA*, nevertheless in only two cases the k value is fair (Table 8).

Test	Inputs							Results	
	B2, B3, B4, B8	EVI	NDVI	VV	VH	angle	Ratio (VH/VV)	*GA* (%)	k
3	x	x	x	x	x	x	x	63	0.54
	x	x	x	x	x	x		59	0.50
	x	x	x	x	x			60	0.51
	x	x	x					58	0.50
	x	x	x	x				61	0.53
	x	x	x		x			53	0.42
	x	x	x			x		54	0.44
	x			x	x	x		61	0.52
	x							50	0.39
		x	x	x	x	x		60	0.50
				x	x	x		36	0.14
				x	x	x	x	36	0.14
						x	x	30	0.00
		x	x			x	x	55	0.43
	x					x	x	55	0.45
4	x	x	x	x	x	x	x	58	0.48
	x	x	x	x	x	x		56	0.47
	x	x	x	x	x			56	0.46
	x	x	x					50	0.40
	x	x	x	x				53	0.43
	x	x	x		x			52	0.41
	x	x	x			x		53	0.43
	x			x	x	x		60	0.52
	x							44	0.32
		x	x	x	x	x		58	0.48
				x	x	x		39	0.18
				x	x	x	x	39	0.18
						x	x	29	0.00
		x	x			x	x	47	0.36
	x					x	x	51	0.41

Table 6. Combination of bands and indices used for the classification with SVM in Scenario 3, along with *GA* and k. 'x'= included

Image	TS1	TS2	TS3
20180926T101021_20180926T101704_T32TPP	x		x
20181021T101039_20181021T101201_T32TPP	x		x
20181115T101251_20181115T101746_T32TPP	x		x
20181225T101421_20181225T101424_T32TPP	x		x
20190104T101411_20190104T101407_T32TPP	x		x
20190223T101021_20190223T101729_T32TPP	x	x	
20190320T101029_20190320T101437_T32TPP	x	x	
20190419T101029_20190419T101030_T32TPP	x	x	
20190613T101031_20190613T101027_T32TPP	x	x	
20190812T101031_20190812T101028_T32TPP	x	x	
20190901T101031_20190901T101134_T32TPP	x	x	

Table 7. Time series of S2 acquired during in the italian agricultural period. 'x'= included

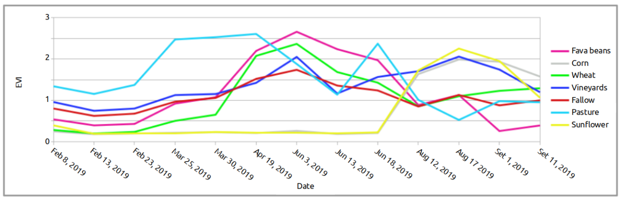

Figure 6. Time series of the median EVI for each sampled class (Scenario 4)

Scenario	Inputs	Time Serie	*GA* (%)	k
RF (number of trees: 10)	Bands and indices	TS1	75.40	0.70
		TS2	74.80	0.70
		TS3	71.90	0.66
SVM (Kernel Type: 'LINEAR'. cost: 10)	Bands and indices	TS1	77.30	0.73
		TS2	77.30	0.73
		TS3	77.30	0.73
RF (number of trees: 10)	Bands	TS1	71.10	0.65
		TS2	68.30	0.61
		TS3	60.20	0.52
SVM (Kernel Type: 'LINEAR'. cost: 10)	Bands	TS1	77.30	0.73
		TS2	70.00	0.64
		TS3	55.50	0.47
RF (number of trees: 15)	Indices	TS1	75.25	0.70
SVM (Kernel Type: 'LINEAR'. cost: 5)	Indices	TS1	75.72	0.71
RF (number of trees: 20)	Indices	TS1	75.14	0.70
SVM (Kernel Type: 'LINEAR'. cost: 3)	Indices	TS1	77.12	0.72

Table 8. Combination of bands and indices used for the classification with SVM in Scenario 4, along with *GA* and k

As already stated in scenario 2, when bands and indices (EVI, SSRG and GRVI) are used in combination the classification accuracy is improved. SVM (kernel type: "LINEAR." Cost: 10) used for the three time series and using either bands and indices was the best performer, reaching GA values higher than 77% and very good *k* values according to the scale of Monserud and Leemans (1992).

The best RF result was 1.9% (*GA*) below the best SVM results, in both cases the *k* degree of agreement is very good.

In the Figure 7 are presented the classification maps belonging to the highest RF and SVM results.

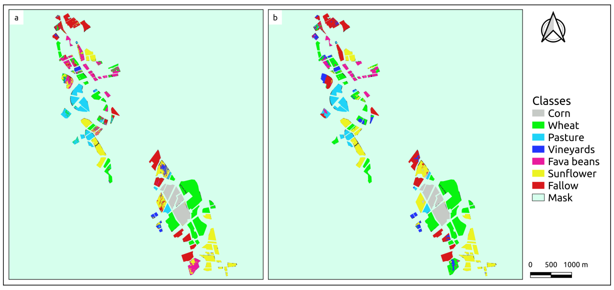

Figure 7. Classified Images in Scenario 4: a) RF (number of trees:10) for the time series number 1 with bands and indices. b) SVM (Kernel Type: 'LINEAR'. cost: 10) for the time series number 1 with bands

4. CONCLUSIONS

In this first approach, the use of Google Earth Engine platform for crop mapping was used in order to asses the performance of different classification algorithms. The results of applying the classifiers in different scenarios in a rural area in center Italy are presented.

The use of scarce field data partially hampered the training of the algorithms.

Among the five classification algorithms (Minimum Distance, Random Forest, Support Vector Machine, Classification and Regression Trees and Naïve Bayes) that were used in the proposed scenarios, the best performers were obtained RF and SVM.

Integrating S1 and S2 slightly improves the classification with respect to only S2 image classification results. On the other hand, the use of time series substantially improves supervised classifications.

A future development of the research is to test the advantages brought by the integration of Sentinel-1 and Sentinel-2 time series.

ACKNOWLEDGEMENTS

To the Institute of Applied Physics "Nello Carrara" (IFAC, CNR) for providing the data for this experience. To the Gulich Institute (CONAE-UNC) for the lessons taught in these two years of Master courses. Also to the "Facultad de Ciencias Agropecuarias (U.N. Córdoba)" for the support and resources received to undertake and complete the Master's degree. Last but not least, to my colleagues Federico Machado and Giuliana Beatriz Beltramone for their advice and contributions to this paper.

References

Bilal, M., Nazeer, M., Nichol, J. E., Bleiweiss, M. P., Qiu, Z., Jäkel, E., Campbell, J. R., Atique, L., Huang, X., Lolli, S., 2019. A Simplified and Robust Surface Reflectance Estimation Method (SREM) for Use over Diverse Land Surfaces Using Multi-Sensor Data. *Remote Sensing*, 11(11), 1344.

Bishop, C. M., 2006. *Pattern recognition and machine learning*. springer.

Breiman, L., 2001. Random forests. *Machine learning*, 45(1), 5–32.

Burges, C. J., 1998. A tutorial on support vector machines for pattern recognition. *Data mining and knowledge discovery*, 2(2), 121–167.

Carrasco, L., O'Neil, A. W., Morton, R. D., Rowland, C. S., 2019. Evaluating combinations of temporally aggregated Sentinel-1, Sentinel-2 and Landsat 8 For land cover mapping with Google Earth Engine. *Remote Sensing*, 11(3), 288.

Dong, J., Xiao, X., Menarguez, M. A., Zhang, G., Qin, Y., Thau, D., Biradar, C., Moore III, B., 2016. Mapping paddy rice planting area in northeastern Asia with Landsat 8 images, phenology-based algorithm and Google Earth Engine. *Remote sensing of environment*, 185, 142–154.

ESA, 2019. SNAP Software, Version 7.0.0. http://step.esa.int/main/download/snap-download/. (Accessed on 10/10/2019).

Fieuzal, R., Baup, F., Marais-Sicre, C., 2013. Monitoring wheat and rapeseed by using synchronous optical and radar satellite data—From temporal signatures to crop parameters estimation. *Advances in Remote Sensing*, 2(02), 162.

Gamon, J., Surfus, J., 1999. Assessing leaf pigment content and activity with a reflectometer. *The New Phytologist*, 143(1), 105–117.

Gorelick, N., Hancher, M., Dixon, M., Ilyushchenko, S., Thau, D., Moore, R., 2017. Google Earth Engine: Planetary-scale geospatial analysis for everyone. *Remote Sensing of Environment*. https://doi.org/10.1016/j.rse.2017.06.031. (Accessed on 09/09/2019).

Haykin, S., 2009. *Neural networks and machine learning*. 3rd edn, Pearson Prentice Hall New Jersey USA.

Italian Confederation of Agriculturist, 2017. Non solo siccità. Il vero dramma dell'agricoltura è un'Italia inefficiente che non risolve i problemi. https://www.ciatoscana.eu/home/non-solo-siccita-vero-dramma-dellagricoltura-unitalia-inefficiente-non-risolve-problemi/. (Accessed on 11/11/2019).

Jog, S., Dixit, M., 2016. Supervised classification of satellite images. *2016 Conference on Advances in Signal Processing (CASP)*, IEEE, 93–98.

Jony, R. I., Woodley, A., Raj, A., Perrin, D., 2018. Ensemble classification technique for water detection in satellite images. *2018 Digital Image Computing: Techniques and Applications (DICTA)*, IEEE, 1–8.

Kumar, P., Gupta, D. K., Mishra, V. N., Prasad, R., 2015. Comparison of support vector machine, artificial neural network, and spectral angle mapper algorithms for crop classification using LISS IV data. *International Journal of Remote Sensing*, 36(6), 1604–1617.

Mardani, M., Mardani, H., De Simone, L., Varas, S., Kita, N., Saito, T., 2019. Integration of Machine Learning and Open Access Geospatial Data for Land Cover Mapping. *Remote Sensing*, 11(16), 1907.

Mathur, A., Foody, G. M., 2008. Crop classification by support vector machine with intelligently selected training data for an operational application. *International Journal of Remote Sensing*, 29(8), 2227–2240.

Mirelva, P., Nagasawa, R., 2019. Application of Sentinel-1 Data for Classifying Croplands Using Google Earth Engine. *International Journal of Geoinformatics*, 15(3).

Monserud, R. A., Leemans, R., 1992. Comparing global vegetation maps with the Kappa statistic. *Ecological modelling*, 62(4), 275–293.

Motohka, T., Nasahara, K. N., Oguma, H., Tsuchida, S., 2010. Applicability of green-red vegetation index for remote sensing of vegetation phenology. *Remote Sensing*, 2(10), 2369–2387.

Müller-Wilm, U., Devignot, O., Pessiot, L., 2019. http://step.esa.int/main/third-party-plugins-2/sen2cor/. (Accessed on 08/09/2019).

Orynbaikyzy, A., Gessner, U., Conrad, C., 2019. Crop type classification using a combination of optical and radar remote sensing data: a review. *international journal of remote sensing*, 40(17), 6553–6595.

Rwanga, S. S., Ndambuki, J., 2017. Accuracy assessment of land use/land cover classification using remote sensing and GIS. *International Journal of Geosciences*, 8(4), 611–622.

Shelestov, A., Lavreniuk, M., Kussul, N., Novikov, A., Skakun, S., 2017. Exploring Google Earth Engine platform for big data processing: Classification of multi-temporal satellite imagery for crop mapping. *frontiers in Earth Science*, 5, 17.

Sistema Informativo Territoriale ed Ambientale, 2019. Regione Toscana: Uso e copertura del suolo. http://www502.regione.toscana.it/geoscopio/usocoperturasuolo.html. (Accessed on 01/08/2019).

Sun, C., Bian, Y., Zhou, T., Pan, J., 2019. Using of Multi-Source and Multi-Temporal Remote Sensing Data Improves Crop-Type Mapping in the Subtropical Agriculture Region. *Sensors*, 19(10), 2401.

Teluguntla, P., Thenkabail, P. S., Oliphant, A., Xiong, J., Gumma, M. K., Congalton, R. G., Yadav, K., Huete, A., 2018. A 30-m landsat-derived cropland extent product of Australia and China using random forest machine learning algorithm on Google Earth Engine cloud computing platform. *ISPRS journal of photogrammetry and remote sensing*, 144, 325–340.

Van Tricht, K., Gobin, A., Gilliams, S., Piccard, I., 2018. Synergistic use of radar Sentinel-1 and optical Sentinel-2 imagery for crop mapping: A case study for Belgium. *Remote Sensing*, 10(10), 1642.

Wu, B., Gommes, R., Zhang, M., Zeng, H., Yan, N., Zou, W., Zheng, Y., Zhang, N., Chang, S., Xing, Q. et al., 2015. Global crop monitoring: a satellite-based hierarchical approach. *Remote Sensing*, 7(4), 3907–3933.

Xiong, J., Thenkabail, P., Tilton, J., Gumma, M., Teluguntla, P., Oliphant, A., Congalton, R., Yadav, K., Gorelick, N., 2017. Nominal 30-m cropland extent map of continental Africa by integrating pixel-based and object-based algorithms using Sentinel-2 and Landsat-8 data on Google Earth Engine. *Remote Sensing*, 9(10), 1065.

https://doi.org/10.5194/isprs-archives-XLII-3-W12-2020-291-2020 | © Authors 2020. CC BY 4.0 License.
Primary publication at IEEE Xplore: https://doi.org/10.1109/LAGIRS48042.2020.9165561